J. Appl. Cryst. (1996). **29**, 7–15

Real-Space Distributions from Small-Angle Scattering Data: Structure Interference Method *versus* Indirect Transformation Method

H. G. KRAUTHÄUSER, W. LENNARTZ AND G. NIMTZ

II Physikalisches Institut, Universität zu Köln, Zülpicher Strasse 77, 50937 Köln, Germany.
E-mail: hgk@arthur.ph2.uni-koeln.de

(Received 8 February 1995; accepted 21 June 1995)

Abstract

The indirect transformation method (program *ITP*) developed by Glatter since 1977 is still one of the most popular methods for obtaining real-space information from small-angle scattering data. In order to validate the novel structure interference method (SIM), a comparison of the two methods has been performed with both simulated and experimental data. Although no explicit smoothing criterion is used in SIM, the solutions are less influenced by oscillations, termination effects are smaller and higher real-space resolution is obtained compared with ITP. It has been found that the structure interference method is very robust even in the case of incomplete data ($h_1 R_{\max} > \pi$) where the indirect transformation method fails to find a physically meaningful solution.

1. Introduction

Small-angle scattering of X-rays or neutrons is often used to get real space information [here, the volume- or number-weighted particle size distribution of the sample; $D_v(R)$ or $D_n(R)$] for mesoscopic systems [a good review is given in the book of Glatter & Kratky (Glatter & Kratky, 1982)]. Only a small amount of information can be deduced from the scattering curve directly. If real-space distributions should be obtained, the inversion of small-angle scattering data becomes an ill-posed problem because the solution is not unique and unstable: the transformation

$$\begin{aligned} T: \text{'real space'} &\xrightarrow{T_1} \text{'Fourier space'} \xrightarrow{T_2} \text{'measuring space'} \\ D(R) &\rightarrow \tilde{I}(h) = T_1 D(R) \rightarrow I(h) \\ &= TD(R) = T_2 T_1 D(R) \end{aligned} \tag{1}$$

is known from scattering theory,* but different distributions $D(R)$ lead to intensities $I(h)$, which fits all to the experimental intensities $I_{\exp}(h)$ within experimental and theoretical errors. Generally, the transformation T is not only determined by scattering theory (T_1), but smearing effects due to camera geometry and wavelength distribution have also to be considered (T_2). The smearing transformation T_2 gives rise to an information loss that makes the evaluation of the scattering curve more difficult.

Glatter's indirect transformation method (often called indirect Fourier transformation; in the following denoted with the name of the program: *ITP*) is a well established method for small-angle scattering-data evaluation (Glatter, 1977*a*,*b*, 1980*a*,*b*; Glatter & Kratky, 1982). The purpose of this paper is to compare the indirect transformation method with the novel structure interference method (SIM) that has been described in more detail elsewhere (Krauthäuser, 1994; Krauthäuser, http://www.rrz.uni-koeln.de/~abb08 and program available by e-mail from the author).

Both methods mentioned here – and also all regularization and maximum entropy methods, (*e.g.* Gull & Skilling, 1984; Hansen & Pedersen, 1991; Moore, 1980; Morrison, Corcoran & Lewis, 1992; Potton, Daniell & Rainford, 1988; Semenyuk & Svergun, 1991; Weese, 1992) – start with an expansion of the real-space distribution with starting functions $\varphi_v(R)$:

$$D_{\mathbf{c}}(R) = \sum_{v=1}^{N} c_v \varphi_v(R) = \mathbf{c} \cdot \boldsymbol{\varphi}(R). \tag{2}$$

For Glatter's *ITP*, these functions are equidistant cubic *b*-spline functions, for SIM, the $\varphi_v(R)$ are the characteristic functions of disjunct intervals $[R_v, R_{v+1}[$:

$$\varphi_v(R) = \begin{cases} 1 & R \in [R_v, R_{v+1}[\\ 0 & \text{else.} \end{cases} \tag{3}$$

Because the transformation T is linear, the scattering intensities $I_{\mathbf{c}}(h)$ for a given set of coefficients c_v can be expressed as

$$\begin{aligned} I_{\mathbf{c}}(h) = TD_{\mathbf{c}}(R) &= \sum_{v=1}^{N} c_v T_2 T_1 \varphi_v(R) \\ &= \sum_{v=1}^{N} c_v T_2 \psi_v(h) = \sum_{v=1}^{N} c_v \chi_v(h) = \mathbf{c} \cdot \boldsymbol{\chi}(h), \end{aligned} \tag{4}$$

* $I(h)$ is the smeared scattering intensity at the scattering vector $h = (4\pi/\lambda)\sin(\Theta)$, λ is the central wavelength of the primary radiation, Θ is half of the scattering angle and $D(R)$ is the real-space distribution.

where the functions $\psi_\nu(h)$ are the theoretical intensities according to the real space functions $\varphi_\nu(R)$ and $\chi_\nu(h)$ are the functions $\psi_\nu(h)$ smeared with the beam profiles and the wavelength distribution. The transformation of a starting function $\varphi_\nu(R)$ into the measuring space is illustrated in Fig. 1 for the case of a dilute system of homogeneous spherical particles and smeared with profiles typical for a Kratky camera. The compatibility of a solution $D_c(R)$ with the experimental intensities $I_{exp}(h)$ is measured by means of the weighted least-squares expression

$$\chi^2 = \sum_{i=1}^{M} (I_{exp}(h_i) - I_c(h_i)/\sigma(h_i))^2, \qquad (5)$$

where M denotes the number of measured points and $\sigma(h_i)$ the (statistical) standard deviation of the intensity $I_{exp}(h_i)$. With the assumption that the data are only affected by the statistical errors $\sigma(h_i)$, a meaningful lower limit for χ^2 is given by M:

$$I_{exp}(h_i) - I_c(h_i) = \pm\, \sigma(h_i) \Rightarrow \chi^2 = M. \qquad (6)$$

Of course, statistics are not the only error source. Other experimental errors (*e.g.* blank scattering correction) and also theoretical errors (*e.g.* an assumption of perfectly spherical scatterers) have to be considered also. Thus, all solutions $D_c(R)$ leading to a χ^2 smaller than M times an approximation grade $\varepsilon \geq 1$ are possible solutions in the sense of a sufficient fit. The set of solutions satisfying the approximation criterion (an N-dimensional ellipsoid, possibly degenerate) can be determined with usual numerical methods (*e.g.* singular-value decomposition). Therefore, from a mathematical point of view the problem is solved but, in practice, the problem is now to select the 'right' solution from this set. But how to select a solution, since the real distribution is unknown? One possibility – and this is done in all regularization methods – is to expand the least-squares condition by an additional condition concerning the shape or the smoothness of the admissible solutions. For the indirect transformation method, this secondary condition is the norm $N_{c'}$ of the first deviation of the coefficients vector (this is the nonsmoothness of the solution):

$$\chi^2 \to \chi^2 + \lambda N_{c'} = \chi^2 + \lambda \sum_{\nu=1}^{N-1} (c_{\nu+1} - c_\nu)^2. \qquad (7)$$

The solutions of the corresponding normal equations are determined by matrix inversion for different Lagrange multipliers λ. The optimal Lagrange parameter is selected from the point of inflection in the so called stability plot – a plot of χ^2 and $N_{c'}$ *versus* λ (Glatter & Kratky, 1982).

2. The structure interference method

In contrast to regularization methods, SIM does not expand the least-squares condition. It only makes use of the demand that a physically meaningful solution has to be independent of the real-space discretization given by

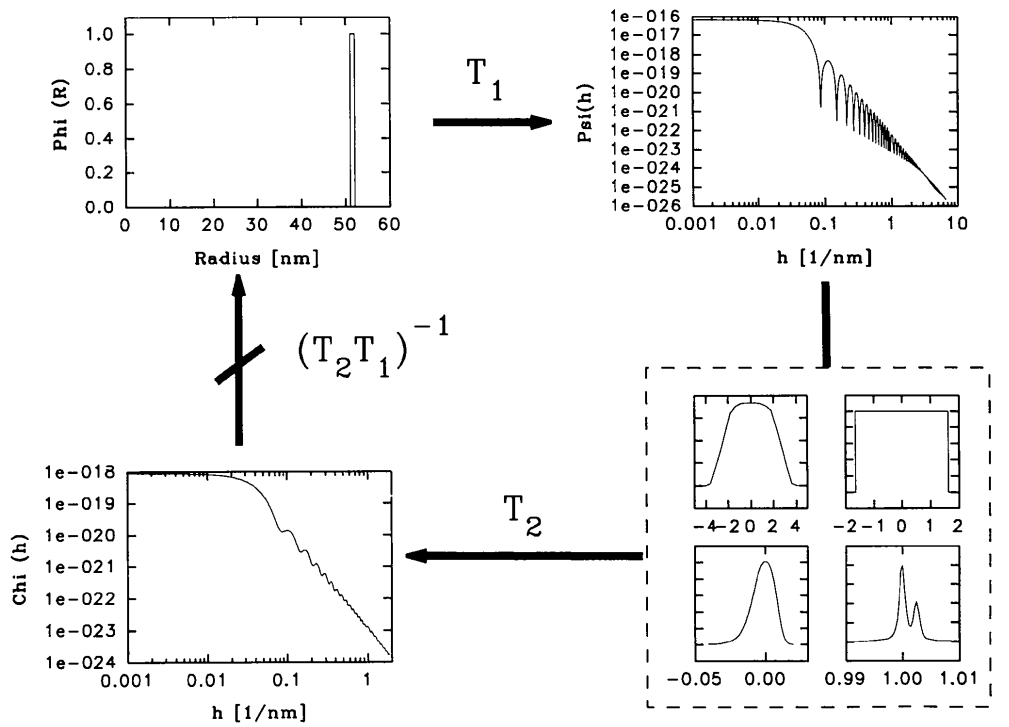

Fig. 1. Transformation of a starting function $\varphi_\nu(R)$ into the 'measuring space' with beam profile typical for a Kratky camera.

the set $\{R_v : v = 1 \ldots N\}$: for every randomly chosen set of R_v a solution can be calculated iteratively by minimization χ^2 until it becomes smaller than an approximation grade ε that must be carefully chosen with respect to the experimental and theoretical errors. In the current implementation of SIM [program *FLOOD* (available by email from the author) (Krauthäuser, http://www.rrz.uni-koeln.de/~abb08)] the minimization is performed using a conjugated gradient algorithm, but other algorithms, *e.g.* genetic algorithms, might be possible also. A suitable approximation grade $\varepsilon = \chi^2/M$ can be determined from a plot of ε and N_c *versus* the number of iterations in the minimization process. A typical example of such a 'trace plot' is shown in Fig. 2: the approximation grade decreases rapidly within the first 15 iterations while the nonsmoothness of the solution increases. After the 15th iteration, both the approximation grade and the nonsmoothness become more constant. From the trace plot of this example, the approximation grade is set to 4 (horizontal line in Fig. 2). Up to now, the determination of the approximation grade has been made 'by hand' as described above from a trace plot, but in principle it will be possible to implement an algorithm that adjusts the approximation grade from the evolution of the solution automatically.

All single solutions for a given discretization show both systematic and unsystematic structures. By averaging of solutions according to different real-space discretizations, a solution is obtained that:

(i) satisfies the approximation criterion;

(ii) shows only the systematic structures of the single solutions.

In Fig. 3, the averaging of single solutions is illustrated for a real scattering system. It has been shown that this very simple algorithm is sufficient to obtain physical meaningful solutions (Krauthäuser, 1994).

The number of single solutions that has to be averaged to obtain sufficient real-space distributions is typically 50–100. Thus, the computation time used to get the final real-space solution is very large, especially if all smearing effects have to be considered. The computation time for an *ITP* solution is approximately the same as for one single SIM solution. In order to overcome the problem of large computation times for the complete SIM solution, the program *FLOOD* has been parallelized, which was a very simple process since the computation of single solutions is absolute independent. Up to now, the program has been used on workstations, workstation clusters (using PVM3), multiprocessor workstations (PVM3) and the massively parallel transputer system Parsytec GCel-3/1024 with 1024 nodes. A comparison of computing times for one single solution for different architectures is given in Table 1. The speed-up with PVM3 is shown in Fig. 4 together with a fit to Amdahl's law that gives a formula for the speed-up for a program with a serial fraction s: Speed-up $= 1/[s + (1 - s)/N] < 1/s$, where N denotes the number of processors. The serial fraction can be obtained from a fit of Amdahl's law to the CPU times for different numbers of processors: $s = 0.01$.

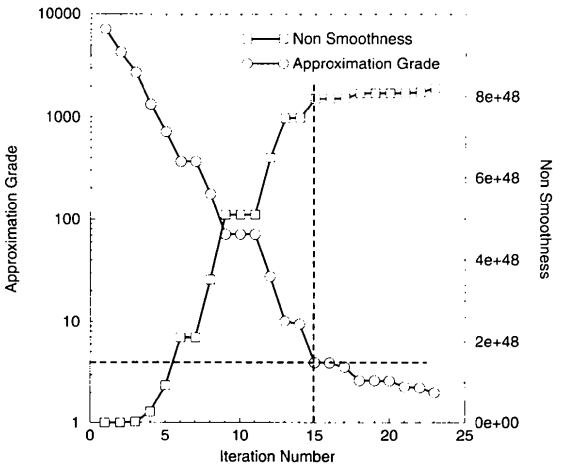

Fig. 2. An example 'trace plot': the approximation grade $\varepsilon = \chi^2/M$ and the 'nonsmoothness' $N_c = \sum_{v=1}^{N-1}(c_{v+1} - c_v)^2$ are plotted *versus* the number of iterations of the minimization process. As described in the text, this plot helps to find an adequate termination criterion for the determination of a single solution.

3. Results

In the following, a direct comparison of the results obtained from both methods is presented. All curves are evaluated with the same or very similar parameters concerning the size range in real space and the real-space discretization. Certainly, the scattering curves, also, the primary data evaluation (blank scattering correction, Porod correction* *etc.*) and the beam profiles used to calculate the smearing have been the same.

3.1. *Real-space discretization*

The code of the program *ITP* was optimized compared with Glatter's original version (double-precision calculation, renunciation of divisions and the power function *etc.*). Owing to this optimization, a higher real-space resolution and smaller computation times have been achieved. One might ask whether these changes are really optimizations. Glatter gives a highest value for the number of spline functions for his original version of

* The final slope of scattering curves is given by Porod's formula $I(h) \propto h^{-x}$ with $x = 4$ for point collimation and $x = 3$ for slit collimation. If the intensities are affected by an additional constant background, this background can be determined from the Porod plot [a plot of $h^x I(h)$ *versus* h^x]. This determination is called Porod correction within this work.

Table 1. *Computation times for different architectures*

All times were obtained for a sample run with typical parameters: slit length and slit width smearing, 100 coefficients in real space (N), 343 measured intensities (M). The computation time is proportional to the product $N \times M$.

System	Processor	CPU time (s)	Index (%)
Linux-PC	Intel 80486DX2 (50 MHz)	671	100
HP9000/720	PA-Risc (50 MHz)	184	365
DEC 7000/640	Alpha (275 MHz)	127	528
HP9000/735	PA-Risc (99 MHz)	94	714
IBM RS/6000-990	RS6000	73	919
Parsytec GCel-3/1024	16 × Inmos T805 (30 MHz)	158	425
Parsytec GCel-3/1024	64 × Inmos T805 (30 MHz)	41	1637
SNI SC900	1 × R8000 (75 MHz)	63	1065
SNI SC900	6 × R8000 (75 MHz)	11	6100
SNI SC900	10 × R8000 (75 MHz)	7	9586

$N \simeq 30$ (Glatter, 1980*b*). In a newer paper dealing with optical sizing of small colloidal particles, Schnablegger & Glatter argue, that 'It is neither necessary nor profitable to use a narrow grid (sampling) for the representation of $D(R)$, since the information content of polydisperse scattering functions is not high'. (Schnablegger & Glatter, 1991). In Fig. 5, the volume-weighted particle-size distribution obtained with *ITP* for a system of 1.1% water in a matrix of butyl rubber (this system will be discussed later in more detail) is illustrated for different numbers of spline functions. For small numbers of splines ($N \leq 50$), the solution is smooth and shows only one structure that starts – depending on the number of splines – below 10 nm and is not fully relaxed to zero even for the last spline. When the number of splines becomes larger than ~ 50, the solutions start to oscillate and two sharp peaks arise, one at each end of the size range. Which of these 'new' structures are real? Obviously, the oscillations are not. A detailed analysis of a whole concentration series of this system [by transmission electron microsopy (TEM), energy-dispersive X-ray fluorescence spectrometry (EDX), wide-angle diffractometry, differential scanning calorimetry (DSC) and broadband complex impedance spectroscopy] shows that it is the first sharp peak that is due to the water in the system (only this structure depends systematically on the water content) and the broad structure – which has been found for small numbers of splines too – has to be assigned to ZnO_2 crystallites in the rubber matrix (this structure does not depend on the water content). The peak at large sizes cannot be assigned to a real structure in the system; it is a termination effect. It must be emphasized that it is impossible to decide that the first peak is real and the other a termination effect without additional knowledge. Also, it has to be emphasized that for this system the most interesting information (about the water) is only available for large numbers of spline functions. Thus, for this system it is necessary and profitable to use a narrow grid for the representation of particle size distributions, but it is also necessary to use a method that can handle this fine grid in real space and that does not produce oscillations or termination effects with increasing real-space resolution.

3.2. *Simulation results*

In simulations, arbitrary real-space distributions can be transformed to the 'measuring space' according to the transformation T. Additionally, any kind of error (noise, constant background *etc.*) can be added to these intensities to simulate experimental conditions. Since the original real-space distribution is known, simulations are an excellent tool to test what amount of information can be retrieved from the simulated 'measuring curve' by a given evaluation program.

First simulation results are presented in Fig. 6. The original distribution ('Cologne Cathedral') is assumed to be a number-weighted particle size distribution of a dilute polydisperse system of homogeneous spheres. The transformation T also includes the smearing transformation with typical beam length, beam width and wavelength distribution profiles. The main characteristics of this distribution that should be resolved by the evaluation program are:

(i) $D_n(R) = 0$ for $R < 16$ nm and $R > 46$ nm;

(ii) three peaks (spires) at 21, 26 and 34 nm.

Before the evaluation using SIM and *ITP*, 1% Gaussian error has been added to the simulated scattering curve.

Fig. 6 shows the original distribution together with the results obtained from SIM and *ITP*. In the SIM solution, all main characteristics of the original distribution are archived. The first two spires began to unify, but they are still separated. The *ITP* solution has only one main peak at the positions of the first two spires and a small shoulder at the position of the third spire. In the range between 0–16 nm, where the original distribution equals zero and, also, the SIM solution shows only little noise around zero, the *ITP* solution has a strong peak to negative values that is not shown in Fig. 6. The plot of the residuals shows that the approximation to the scattering intensities is significantly worse for the *ITP* solution. *ITP* solutions with smaller Lagrange multipliers give a better approximation but the

real-space solutions are strongly oscillating (there is no clear point of inflection in the stability plot for this simulation; the *ITP* solution shown here is that looking most similar to the original distribution).

The results of an other simulation are presented in Fig. 7. This example has been performed as a blind test: one of the authors has done the simulation with a distribution chosen by him and added noise (1% Gaussian error) and a constant background to the simulated 'scattering curve'. Then, the evaluation for this data has been performed with SIM and *ITP* by another author without knowledge concerning the original distribution except that the largest radius (particle size) is 100 nm. The background has been determined from a Porod plot.

The original distribution does not consist of one compact structure but an extended structure in the middle of the particle size range is flanked by two very sharp structures, one at each end of the size range that could be investigated in real small-angle X-ray experiments using a Kratky camera. Because the scattering intensity is proportional to the sixth power of the particle radius, the question is whether the structures at smaller particle sizes could be obtained from the scattering curve or not. Another difficulty comes with the h range of the simulated data: the smallest scattering vector for the given data set is $h_1 \simeq 0.06\ \mathrm{nm}^{-1}$. Therefore, the scattering curve contains the full information only for particles with $R < \pi/h_1 \simeq 52$ nm, which is very small compared to the size range in the original distribution.

Looking at the solutions in Fig. 7, one must conclude that *ITP* does not work for this example. The solution produced with *ITP* gives a structure at ~20 nm, where nothing is seen in the original distribution. The middle part of the *ITP* distribution is characterized by a strong oscillation and even the contribution at large sizes is far from the original distribution. The SIM solution gives a better result: the two narrow peaks at both ends of the particle size range are reproduced in their positions, but they have become broader. Also, the size and the asymmetry of the structure in the middle is archived. Only one small structure between 70 and 80 nm arises in the SIM solution that does not appear in the original distribution. It is very astonishing that the slope of the residuals for both methods is quite similar over the range of scattering vectors since the real-space distributions look absolutely different.

One might argue that both examples presented here are far from realistic, since 1% statistical error for the whole range of scattering vectors is not to be reached in real experiments and the original distributions have structures that are much sharper than is usual in real systems.

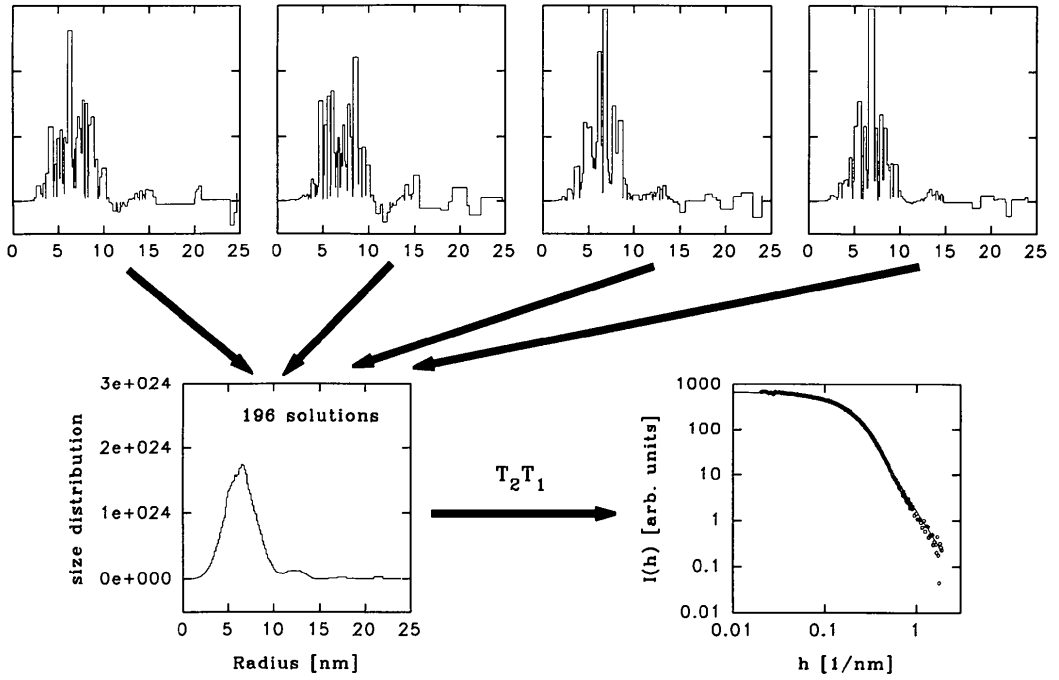

Fig 3. Single solutions according to different real-space discretizations (upper graphs) show both systematic and unsystematic structures. In the averaged solution (lower left graph), only systematic structures are archived. The compatibility of the scattering intensities according to the averaged solution (line in the lower right graph) with the measured intensities (points in the lower right graph) is very good over the whole measuring range.

However, the aim of these simulations is not to model reality. It is more essential to use simulations to test the behaviour of a given algorithm particularly in very extreme situations. The abilities of the two methods to deal with data are compared in the following section.

3.3. *Water in butyl rubber*

Figs. 8 and 9 show the volume-weighted particle size distributions according to the first two points of a concentration series of water in butyl rubber (investigations on very similar systems have been published by Pelster, Kops, Nimtz, Enders, Kietzmann, Pissis, Kyritsis & Woermann, 1993). The measurements were performed with a Kratky camera.

Fig. 8 shows the results for the dry rubber (0% water). For this system, SIM and *ITP* both produce two structures in the range of small particles ($R < 20$ nm). The structure at larger sizes was identified as ZnO_2 crystallites by TEM, EDX and wide-angle diffractometry. Particles that could be assigned to the structure at small sizes are found in the TEM pictures too, but an identification with EDX was impossible because of their small size.* The position of the first structure is shifted to smaller sizes in the *ITP* result. From the TEM pictures, the larger size of the SIM solution has been confirmed. In the region from 20 to 45 nm, it is impossible to decide whether the *ITP* or the SIM solution is closer to the unknown real distribution. No structure has been found in the TEM pictures that could be assigned to the strong

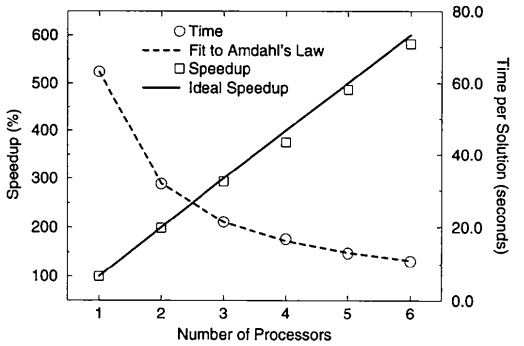

Fig. 4. Speed-up and time per solution for different numbers of processors on a multiprocessor workstation (SNI900) using PVM3. The speed-up is nearly linear. The serial part of the algorithm is determined to 1% from a fit to Amdahl's law.

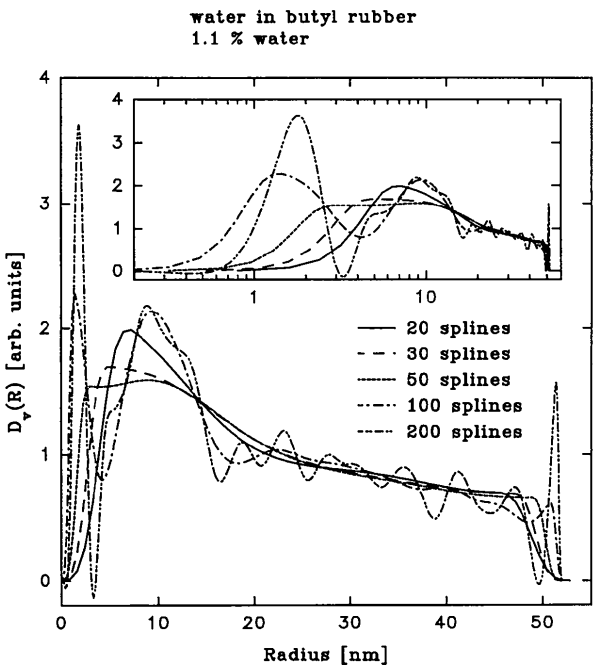

Fig. 5. Comparison of the *ITP* solutions for different numbers of splines. The inset shows the same data but with logarithmic scaling of the x axis.

* Possibly, these structures correspond to carbon or sulfur clusters that are embedded in the rubber matrix.

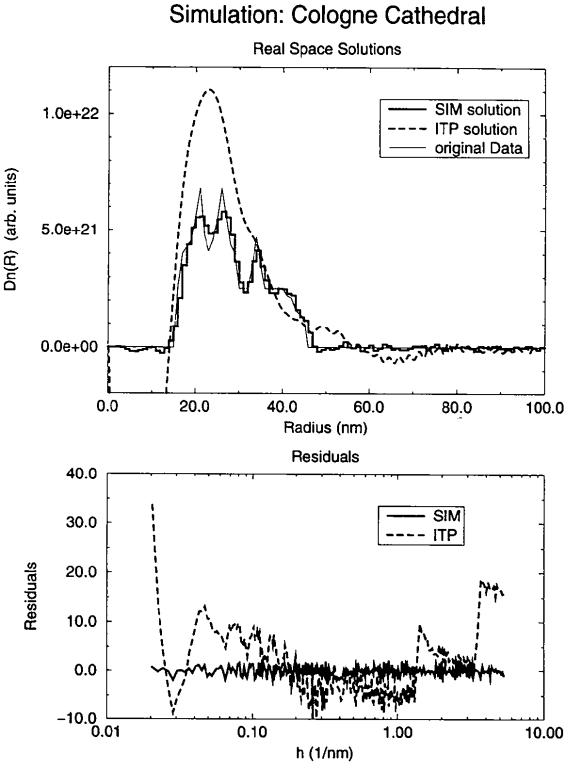

Fig. 6. Comparison of SIM and *ITP* solutions with the original real-space distribution. (*a*) Number-weighted particle-size distribution $D_n(R)$ *versus* particle radius R. (*b*) Residuals $[I_{exp}(h) - I_c(h)]/\sigma(h)$ *versus* magnitude of the scattering vector, h.

peak at the end of the *ITP* solution. Probably, this is a termination effect. The plot of the residuals shows that the approximation to the scattering data is similar for both methods.

Fig. 9 shows the distributions for 1.1% water in the same piece of butyl rubber. The first structure, which has increased by a factor of ~ 3.5 compared to dry rubber, can be assigned to water droplets, which have nearly the same size as the (not clearly identified) scatterers in the dry rubber. Although the water concentration is low and the electron-density contrast between water and butyl rubber is small, the water droplet conceals the structure seen in the dry rubber.

The comparison of the results obtained with *ITP* and SIM is very similar to that of dry rubber: good agreement is obtained for the first two structures, in the outer part the deviation becomes greater and the *ITP* solution shows a strong termination effect. As before, the approximation to the scattering data is very similar for both methods.

3.4. *Indium in oil*

The system 'indium in oil' has been investigated in a recently published paper using the indirect transformation method (Krauthäuser, Heitmann, Kops & Nimtz, 1994). Now, the evaluations have been redone using the structure interference method. In Fig. 10, the SIM solution for a system of 1.2vol.% indium is presented, together with the ITP solution and the results of a TEM analysis, made at the Fraunhofer Institut für angewandte Materialforschung (IFAM) at Bremen.

The agreement between the most probable particle sizes obtained from SIM and from TEM is perfect. Comparing *ITP* and TEM, a clear deviation has to be mentioned. Although no size distribution could be deduced from the TEM pictures because the number of particles was too small, it is obvious that the strong contributions in the *ITP* solution for particle sizes smaller than 5 nm are not real. The residuals are similar for the two methods.

4. Conclusions

It has been shown that the structure interference method is a fully adequate alternative to Glatter's indirect transformation method to obtain particle size distributions from small-angle scattering data. For both simulated and experimental data, the *ITP* solutions show contributions that could not be assigned to real structures. In the volume weighted size distributions investigated above, *ITP* and SIM are closer together as for the number

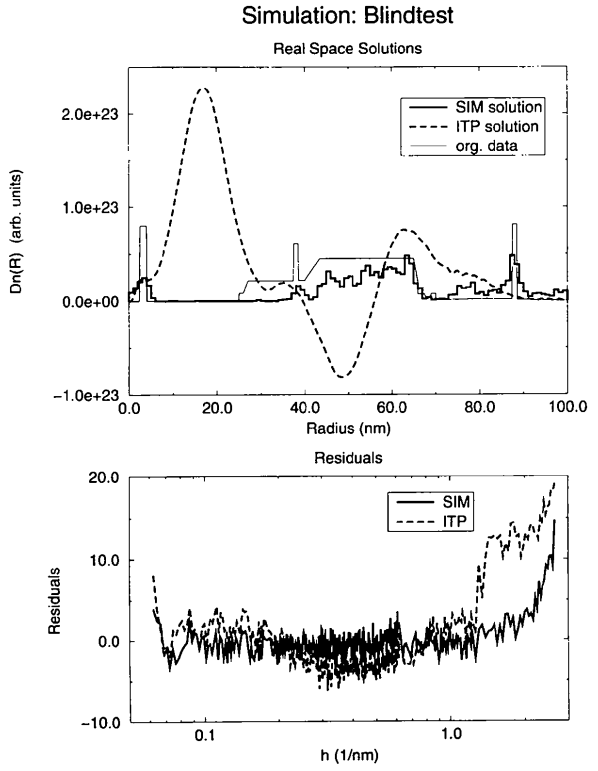

Fig. 7. Comparison of SIM and *ITP* solutions with the original real-space distribution. (*a*) Number-weighted particle-size distribution $D_n(R)$ *versus* particle radius R. (*b*) Residuals $[I_{exp}(h) - I_c(h)]/\sigma(h)$ *versus* magnitude of the scattering vector, h.

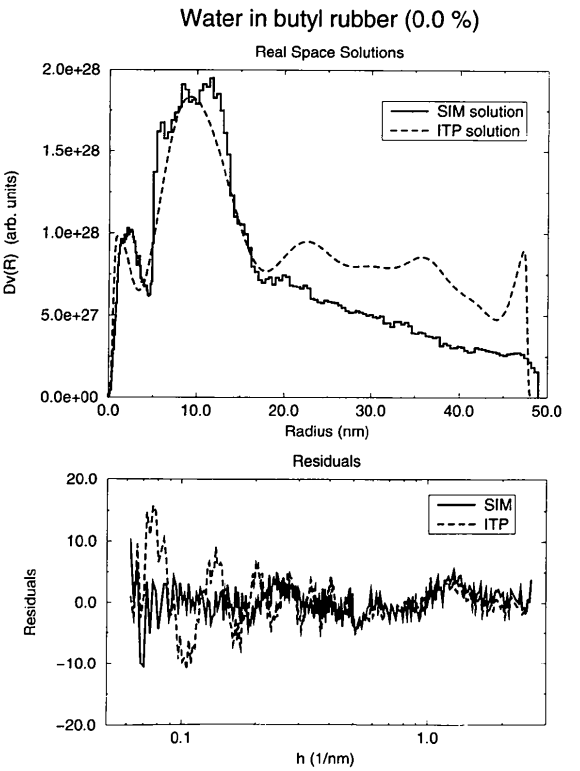

Fig. 8. SIM and *ITP* solutions for dry butyl rubber. (*a*) Volume-weighted particle-size distribution $D_v(R)$ *versus* particle radius R. (*b*) Residuals $[I_{exp}(h) - I_c(h)]/\sigma(h)$ *versus* magnitude of the scattering vector, h.

weighted size distributions, but the *ITP* solution is strongly influenced by termination effects. Thus, the interpretation of the *ITP* solution is more difficult.

The structure interference method can be used with a very fine grid in real space and with an increasing number of functions in real space more information can be resolved from the scattering data. In contrast to SIM solutions, the information gain for the *ITP* solutions with increasing resolution is very poor, since strong oscillations influence the distributions and termination effects occur that could not be distinguished from real structures without additional information.

In the case of incomplete data (Fig. 7), the *ITP* solution has strong negative contributions that are not physically meaningful. Probably, every user would reject such solutions and it would be considered that *ITP* had failed on that data set. Possibly, the introduction of a positivity constraint would produce better *ITP* solutions, but up to now that has not been implemented in the *ITP* program [it has been implemented in Glatter's program for light scattering evaluation (Schnablegger & Glatter (1991) and it is in planned to implement it in ITP].

The main disadvantage of SIM is the computation time. But even if only PCs are available, it is possible to reach acceptable computation times by building a virtual parallel computer from the PCs using PVM3 and a multitasking operating system such as Linux.

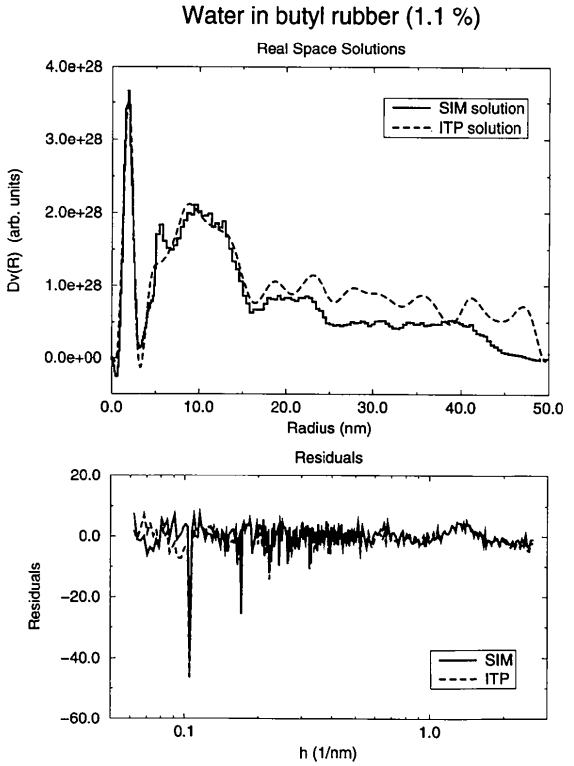

Fig. 9. SIM and *ITP* solutions for 1.1% water in butyl rubber. (*a*) Volume-weighted particle-size distribution $D_v(R)$ *versus* particle radius R. (*b*) Residuals $[I_{exp}(h) - I_c(h)]/\sigma(h)$ *versus* magnitude of the scattering vector, h.

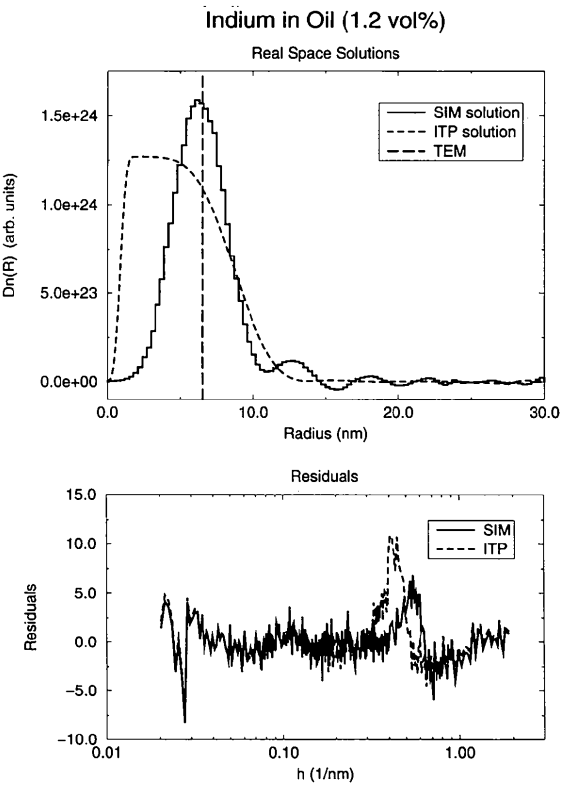

Fig. 10. SIM and *ITP* solutions for 1.1vol.% indium particles in oil. (*a*) Number-weighted particle-size distribution $D_n(R)$ *versus* particle radius R. (*b*) Residuals $[I_{exp}(h) - I_c(h)]/\sigma(h)$ *versus* magnitude of the scattering vector, h.

The authors gratefully acknowledge Dr Brück (BAYER AG, Leverkusen) for preparation of the butyl rubber samples and Professor Dr Woermann (Institut für Physikalische Chemie, Köln) for the supply with equipment for sample preparation. The research was sponsored by the Bundesministerium für Forschung und Technologie (Project 03M 2737B2), the Deutsche Forschungsgemeinschaft (Project Ni-149/22) and the Volkswagen-Stiftung (Project I/65 356).

References

Glatter, O. (1977*a*). *Acta Phys. Austriaca*, **47**, 83–102.
Glatter, O. (1977*b*). *J. Appl. Cryst.* **10**, 415–421.
Glatter, O. (1980*a*). *J. Appl. Cryst.* **13**, 7–11.
Glatter, O. (1980*b*). *J. Appl. Cryst.* **13**, 577–584.
Glatter, O. & Kratky, O. (1982). *Small Angle X-ray Scattering*. New York: Academic Press.
Gull, S. F. & Skilling, J. (1984). *IEE Proceedings*, **131**, *F*6, 646–659.
Hansen, S. & Pedersen, J. S. (1991). *J. Appl. Cryst.* **24**, 541–548.
Krauthäuser, H. G., Heitmann, W., Kops, A. & Nimtz, G. (1994). *J. Appl. Cryst.* **27**, 558–562.

Krauthäuser, H. G. (1994). *Physica (Utrecht) A*, **211**, 317–326.
Moore, P. B. (1980). *J. Appl. Cryst.* **13**, 168–175.
Morrison, J. D., Corcoran, J. D. & Lewis K. E. (1992). *J. Appl. Cryst.* **25**, 504–513.
Pelster, R., Kops, A., Nimtz, G., Enders, A., Kietzmann, H. Pissis, P., Kyritsis, A. & Woermann, D. (1993). *Ber. Bunsenges. Phys. Chem.* **97**, 666–675.
Potton, J. A., Daniell, G. J. & Rainford, B. D. (1988). *J. Appl. Cryst.* **21**, 891–897.
Schnablegger, H. & Glatter, O. (1991). *Appl. Opt.* **30**, 4889–4896.
Semenyuk, A. V. & Svergun, D. I. (1991). *J. Appl. Cryst.* **24**, 537–540.
Weese, J. (1992). *Comput. Phys. Commun.* **69**, 99–111.